Physics and Mathematics of Nonlinear Phenomena 2013 (PMNP2013) IOP Publishing
Journal of Physics: Conference Series **482** (2014) 012033 doi:10.1088/1742-6596/482/1/012033

Two-circles theorem, q-periodic functions and entangled qubit states

Oktay K. Pashaev

Department of Mathematics, Izmir Institute of Technology, Gulbahce Campus, Izmir, Urla 35430, Turkey

E-mail: oktaypashaev@iyte.edu.tr

Abstract. For arbitrary hydrodynamic flow in circular annulus we introduce the two circle theorem, allowing us to construct the flow from a given one in infinite plane. Our construction is based on q-periodic analytic functions for complex potential, leading to fixed scale-invariant complex velocity, where q is determined by geometry of the region. Self-similar fractal structure of the flow with q-periodic modulation as solution of q-difference equation is studied. For one point vortex problem in circular annulus by fixing singular points we find solution in terms of q-elementary functions. Considering image points in complex plane as a phase space for qubit coherent states we construct Fibonacci and Lucas type entangled N-qubit states. Complex Fibonacci curve related to this construction shows reach set of geometric patterns.

1. Introduction

1.1. Method of Images

The problem of vortex images in circular annulus was formulated by Poincare [1] and solved by q-elementary functions in [2]. It was shown that all images are ordered in geometric progression and are determined by singularities of q-logarithmmic and q-exponential functions. By this approach we solved one and two vortex problems in circular annulus [3] and found regular polygon type N vortex configurations [2]. In the present paper we are generalizing these results by studying arbitrary hydrodynamic flow in annular domain bounded by two concentric circles. We formulate general two circle theorem and find self-similar structure of the flow. Then we describe the method of images implications for quantum qubit states.

1.2. Two dimensional stationary flow

Incompressibility condition $div\,\vec{u} = 0$ gives $u_1 = \varphi_x$, $u_2 = \varphi_y$, where $\varphi(x, y)$ is the velocity potential. From irrotational condition $rot\,\vec{u} = 0$ we have $u_1 = \psi_y$, $u_2 = -\psi_x$, where $\psi(x, y)$ is the stream function. They satisfy the Cauchy-Riemann equations $\varphi_x = \psi_y$, $\varphi_y = -\psi_x$. Then the complex potential $f(z) = \varphi + i\psi$ is analytic function $\frac{\partial}{\partial \bar{z}} f(z) = 0$, $z = x + iy$, while the complex velocity $\bar{V}(z) = \frac{\partial}{\partial z} f(z)$ is anti-analytic.

1.2.1. Point vortex The point vortex corresponds to complex potential with logarithmic singularity $f(z) = \frac{\Gamma}{2\pi i} Log(z - z_0)$ and complex velocity with simple pole singularity $\bar{V} = \frac{\Gamma}{2\pi i} \frac{1}{z - z_0}$. Residue at this singularity determines the vortex strength $\Gamma = \oint \vec{u} d\vec{s}$.

1.3. Hydrodynamic flow in bounded domain
For a domain bounded by curve C the problem is to find analytic function $F(z)$ with boundary condition

$$\Im F|_C = \psi|_C = 0,$$

where ψ is the stream function. Then the normal velocity vanishes at boundary $v_n|_C = 0$. For one circle C: $z\bar{z} = r_1^2$ the last condition gives $(\bar{V}(z)z + V(\bar{z})\bar{z})|_C = 0$.

1.4. Milne-Thomson's one circle theorem
For a given flow in plane with complex potential $f(z)$, introduction of boundary circle at the origin C: $|z| = r$ produces the flow with complex potential [4]

$$F(z) = f(z) + \bar{f}\left(\frac{r^2}{z}\right)$$

and complex velocity

$$\bar{V}(z) = u_1 - iu_2 = \bar{v}(z) - \frac{r^2}{z^2}\, v\left(\frac{r^2}{z}\right).$$

1.4.1. Circle theorem for point vortex For the vortex at z_0 with strength ($\Gamma = -2\pi\kappa$) it gives

$$\bar{V}(z) = \frac{i\kappa}{z - z_0} - \frac{i\kappa}{z - \frac{r_1^2}{\bar{z}_0}} + \frac{i\kappa}{z},$$

where the second term describing vortex $-\kappa$ at the inverse point $r_1^2/\bar{z}_0$ to the circle, is the vortex image. The last term as vortex $+\kappa$ at the origin cannot be fixed by the boundary.

1.4.2. Symmetry The above theorem admits the exterior - interior symmetry. If we denote $g(z) \equiv \bar{f}\left(\frac{r^2}{z}\right)$ - potential of interior flow, then $\bar{g}\left(\frac{r^2}{z}\right) = f(z)$ becomes potential of exterior flow so that

$$F(z) = f(z) + \bar{f}\left(\frac{r^2}{z}\right) = g(z) + \bar{g}\left(\frac{r^2}{z}\right)$$

This symmetry allows one to extend results to the problem inside of circular domain.

1.5. Double connected domain
Due to the Riemann mapping theorem, the unit disk can be mapped conformally onto any simply connected region in the plane. This is why the Milne-Thomson one circle theorem allows one to solve the problem for wide class of contours in simply connected domain.

However extension to multiply connected domains is not straightforward. A doubly connected domain can be conformally mapped to annular region $r_1 < |z| < r_2$ uniquely up to linear map,

$$r_2/r_1 = r_2'/r_1' \equiv \sqrt{q}$$

2. Two circles theorem

For annular domain, $r_1 < |z| < r_2$, between two concentric circles $C_1 : |z| = r_1$, $C_2 : |z| = r_2$ the complex potential is

$$F_q(z) = f_q(z) + \bar{f}_q\left(\frac{r^2}{z}\right),$$

where $q = \frac{r_2^2}{r_1^2}$, $f_q(z) = \sum_{n=-\infty}^{\infty} f(q^n z)$ is flow in even annular domains, $\bar{f}_q\left(\frac{r^2}{z}\right) = \sum_{n=-\infty}^{\infty} \bar{f}\left(q^n \frac{r^2}{z}\right)$ is the flow in odd annular domains (see Figure 1).

Proof: By shifting summation index it is easy to show that [7] $Im\, F(z)|_{C_1} = 0$ and $Im\, F(z)|_{C_2} = 0$.

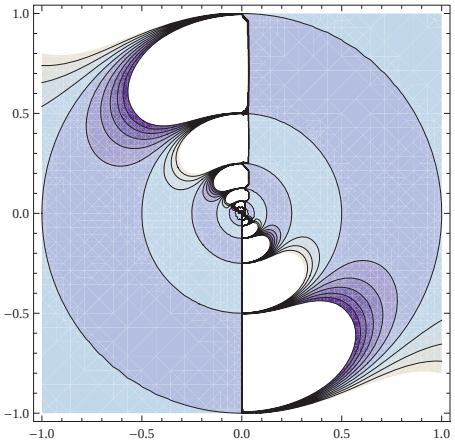

Figure 1. q-periodic flow.

2.1. q-periodicity

From above definition follows that $f_q(qz) = f_q(z)$ which implies that complex potential is q-periodic function $F_q(qz) = F_q(z)$ and

$$D_z f_q(z) \equiv \frac{f_q(qz) - f_q(z)}{(q-1)z} = 0. \tag{1}$$

Corresponding complex velocity

$$\bar{V}(z) = \sum_{n=-\infty}^{\infty} q^n \bar{v}(q^n z) - \frac{r_1^2}{z^2} \sum_{n=-\infty}^{\infty} q^n v(q^n r_1^2 z),$$

then is the q-scale invariant function

$$\bar{V}(qz) = q^{-1} \bar{V}(z).$$

2.2. Jackson complex q-Integral Representation

By definition

$$\int f(z) d_q z \equiv (1-q) z \sum_{n=0}^{\infty} q^n f(q^n z)$$

we get the next representation for our two circle potential

$$F(z) = \frac{1}{1-q} \int \frac{f(z) + \bar{f}(r_1^2/z)}{z} d_q z + \frac{q}{q-1} \int \frac{f(z) + \bar{f}(r_1^2/z)}{z} d_{1/q} z - f(z) - \bar{f}\left(\frac{r_1^2}{z}\right).$$

3. q scale-invariant analytic fractal

For any complex valued function of two variables $f(x,y)$ we define q-differential $d_q f(x,y) = f(qx,qy) - f(x,y)$, expressible by complex q-derivatives (see definition in (1)) as

$$d_q f(x,y) = d_q z\, D_z f(x,y) + d_q \bar{z}\, q^{z\frac{d}{dz}}\, D_{\bar{z}} f(x,y).$$

If function $f(x,y)$ is complex analytic function $\partial_{\bar{z}} f = 0$ then $D_{\bar{z}} f = 0$ and $d_q f(x,y) = d_q z\, D_z f(x,y)$. If in addition the analytic function is scale invariant $f(qz) = q^d f(z)$ then it satisfies the q-difference equation

$$D_z f(z) = \frac{f(qz) - f(z)}{(q-1)z} = \frac{(q^d - 1)}{(q-1)z} f(z) \tag{2}$$

or

$$z D_z f(z) = [d]_q f(z), \tag{3}$$

where $[n]_q = \frac{q^d - 1}{q-1}$ is q-number. General solution of this equation has the following form

$$f(z) = z^d A_q(z), \tag{4}$$

where $A_q(qz) = A_q(z)$ is q-periodic function playing the role of q-periodic modulation.

3.1. Weierstrass-Mandelbrot Function

Well known classical example of continuous but anywhere non-differentiable function

$$W(t) = \sum_{n=-\infty}^{\infty} q^{-nd}(1 - \cos q^n t)$$

$0 < d < 1$, $q > 1$ is a fractal with dimension $2 - d$. It is self-similar $W(qt) = q^d W(t)$ and satisfies q-difference equation $t D_t W(t) = [d]_q W(t)$ similar to considered above [5]. Decomposition $W(t) = t^d A_q(t)$, then gives q-periodic part $A_q(qt) = A_q(t)$ as

$$A_q(t) = \sum_{n=-\infty}^{\infty} q^{-nd} t^{-d}(1 - e^{iq^n t}).$$

Analytic extension of this result to complex domain as in previous section gives analytic fractal in plane.

3.2. Elliptic functions

Let $F(qz) = F(z)$ is analytic q-periodic function. We take arbitrary positive number ω and define pure imaginary number ω' [9] so that $q = e^{2\pi i \frac{\omega'}{\omega}}$ and new function

$$F(z) \equiv \phi\left(\frac{\omega}{\pi i} \ln z\right).$$

Then due to q-periodicity this function is periodic $\phi(u + 2\omega') = \phi(u)$ where $u \equiv \frac{\omega}{\pi i} \ln z$. Another period is related with rotation on 2π around origin $\phi(u + 2\omega) = \phi(u)$. Thus $\phi(u)$ is double-periodic function with periods 2ω, $2\omega'$. To construct this function we need to fix its singular points.

3.3. q-periodic flow

Simplest q-periodic function is

$$f(z) = z^{\frac{2\pi i}{\ln q}} = e^{\frac{2\pi i}{\ln q}\ln z},$$

the principal branch of which is analytic in complex plain with a branch cut along the negative real axis, and $f(qz) = f(z)$. In polar coordinates $z = re^{i\varphi}$ it gives the flow

$$f(z) = e^{-\frac{2\pi}{\ln q}\varphi}(\cos\frac{2\pi}{\ln q}\ln r + i\sin\frac{2\pi}{\ln q}\ln r)$$

with the stream function

$$\psi(x,y) = e^{-\frac{2\pi}{\ln q}\varphi}\sin\left(\frac{2\pi}{\ln q}\ln r\right). \tag{5}$$

The flow has self-similar velocity

$$\bar{V}(z) = \frac{df}{dz} = \frac{2\pi i}{\ln q}\frac{1}{z}e^{\frac{2\pi i}{\ln q}\ln z}$$

and can be interpreted as q-periodically modulated point vortex at origin with strength $\Gamma = -4\pi^2/\ln q$. It is plotted in Figure 1.

The stream function (5) vanishes $\psi|_C = 0$ when $\sin\frac{2\pi}{\ln q}\ln r = 0$, and $\frac{2\pi}{\ln q}\ln r = \pi n$, $n = 0, \pm1, \pm2...$, which determines the set of concentric circles with radiuses ordered in geometric series $r_n = q^{\frac{n}{2}}$. The flow is circular along these circles (see Figure 1). For $n = 0$ we have unit circle at the origin. Then every pair of circles $r_{+k} = q^{k/2}$ and $r_{-k} = 1/q^{k/2}$ is symmetric with respect to the unit circle $r_{-k}\, r_{+k} = 1$. Moreover, for any chosen circle with radius $r_s = q^{s/2}$, exists infinite set of symmetric circles with radiuses $R_k = r_s\, q^{k/2}$ and $r_k = r_s/q^{k/2}$ so that $R_k\, r_k = r_s$. In addition every circle R has the symmetric one r with respect to r_s. Indeed, let $R = q^{n/2}$. Then exist integer numbers $k = n - s$ and $m = s - k$ such that $R = q^{\frac{s+k}{2}}$ and $r = q^{\frac{s-k}{2}}$ satisfy equation $R\, r = r_s$.

From above consideration follows that $f(z) = z^{\frac{2\pi i}{\ln q}}$ describes the hydrodynamic flow in circular annulus with radiuses $r = 1$ and $R = \sqrt{q}$, so that $q = R^2/r^2$. In fact it describes also the flow in any annulus with $r = q^{n/2}$ and $R = q^{m/2}$, but simplest one is when $n = 0$ and $m = 1$. Taking power of this function we get more general set of functions $f^{(N)}(z) = z^{\frac{2\pi i}{\ln q}N}$, where $N \in Z$. This function is q-periodic and in addition $q^{1/N}$-periodic. The stream function vanishes on circles C: $|z|^2 = q^{n/N}$, $n = 0, \pm1, \pm2, ...$, which are symmetric with respect to unit circle. For the set of numbers n multiple N:$n = kN$, where $k = 1, 2...$, circles $r_{+k} = q^{k/2N}$ and $r_{-N} = q^{-k/2N}$ are symmetric and coincides with $N = 1$ case. With growing N we have more and more dense set of geometric circles, splitting the plane on circular annuluses. Combining superposition of these functions we have more general q- periodic function

$$F(z) = \sum_{N=-\infty}^{\infty} a_N\, z^{\frac{2\pi i}{\ln q}N} \tag{6}$$

describing flow in circular annulus $r = 1$, $R = \sqrt{q}$.

3.4. Application to vortex in annular domain

By our Two Circle Theorem for one vortex in annular domain we find

$$F(z) = \frac{\Gamma}{2\pi i}\sum_{n=-\infty}^{\infty}\ln\frac{z - z_0 q^n}{z - \frac{r_1^2}{\bar{z}_0}q^n}.$$

This function is q-periodic $F(qz) = F(z)$ and can be represented in terms of double periodic functions $F(z) \equiv \varphi(\ln(z))$. Explicit expression in terms of elliptic functions was given in [2].

The corresponding velocity potential

$$\bar{V}(z) = \frac{\Gamma}{2\pi i} \sum_{n=-\infty}^{\infty} \left[\frac{1}{z - z_0 q^n} - \frac{1}{z - \frac{r_1^2}{\bar{z}_0} q^n} \right] \tag{7}$$

is scale-invariant analytic function $\bar{V}(qz) = q^{-1}\bar{V}(z)$ and can be represented as $\bar{V}(z) = \frac{\Gamma}{2\pi i\, z} A_q(z)$, where $A(qx, qy) = A(x, y)$ is q-periodic function of two arguments. The last representation shows that the problem looks like q-periodic modulation of one vortex at the origin. Then from our solution we have q-periodic function as

$$A(z) = \sum_{n=-\infty}^{\infty} \left[\frac{z}{z - z_0 q^n} - \frac{z}{z - \frac{r_1^2}{\bar{z}_0} q^n} \right].$$

3.4.1. Pole singularities and vortex images This expression has pole singularities at $z_0\, q^n$, and at symmetric points $\frac{r_1^2}{\bar{z}_0} q^n$, where $n = 0, \pm 1, \pm 2, ...$ For $q > 1$, $0 < |z| < q$ by q-logarithm function [2]

$$\ln_q(1 + z) = \sum_{n=1}^{\infty} \frac{(-1)^{n-1} z^n}{[n]} = (q - 1) \sum_{n=1}^{\infty} \frac{z}{q^n + z},$$

with infinite set of pole singularities at $z = -q^n$, n = 1,2,... then we get expression

$$A(z) = \frac{z}{z - z_0} + \frac{1}{(q - 1)} \left[\ln_q \left(1 - \frac{z}{z_0} \right) - \ln_q \left(1 - \frac{z\bar{z}_0}{r_1^2} \right) + \ln_q \left(1 - \frac{r_2^2}{z\bar{z}_0} \right) - \ln_q \left(1 - \frac{z_0}{z} \right) \right].$$

4. q-scale invariant quantum fractal

As known in Fock-Bargmann representation any vector of quantum state $|\psi >$ is associated in one-to-one correspondence with entire analytic function $\psi(z)$. This function is a wave function

$$< z|\psi >= e^{-|z|^2/2} \psi(\bar{z})$$

in the Glauber coherent state basis $|z >$. The dilatation operator q^N acts on this function as

$$q^{z\frac{d}{dz}} \psi(z) = \psi(qz).$$

It was shown in [10], [11] that this operator produces the q-deformation process associated with fractal generation process and is equivalent to the squeezing transformation. The q-number operator $[N]_q = \frac{q^N - 1}{q - 1}$ in this representation becomes $[z\frac{d}{dz}]_q = \frac{q^{z\frac{d}{dz}} - 1}{q - 1} = zD_z$ so that q-difference equation (3) for scale invariant wave function $\psi(z)$, represents the eigenvalue equation for scale invariant quantum state $|\psi >$,

$$[N]_q|\psi >= [n]_q|\psi > .$$

The general solution of this equation (4) can be considered as descriptive of quantum q-scale invariant fractal. This implies that with hydrodynamic problems discussed in the first part of this paper we can associate quantum states in the Fock-Bargmann representation. Then to the flow in bounded domain determined by the set of images, we introduce the "image" quantum states. These states for one and two circles are given by pairs of symmetric quantum states. One set of images is given by q-deformation of state $|\psi >$: $|q\psi >$, $|q^2\psi >$,... and corresponds

to even number of inversions in the circles. Another set of images is related with odd number of inversions: $|\frac{1}{\psi}>$, $|q\frac{1}{\psi}>$,... To understand structure of elementary inversion state, in next section we study quantum "image" states for $SU(2)$ coherent states, in stereographic projections of qubits. The full construction of q-scale-invariant quantum states as in two circle theorem is under investigation.

5. Mobius transformation and qubit

In this part we apply method of images to construct a set of multiple qubit coherent states. Qubit as a unit of quantum information, can be ascribed to arbitrary point in extended complex plane. Linear transformation

$$\begin{pmatrix} w_1 \\ w_2 \end{pmatrix} = \begin{pmatrix} a & b \\ c & d \end{pmatrix} \begin{pmatrix} \psi_1 \\ \psi_2 \end{pmatrix}$$

acts on homogeneous coordinates $\psi = \psi_1/\psi_2$, $w = w_1/w_2$ by Möbius Transformation

$$w = \frac{a\psi + b}{c\psi + d}, \quad ad - bc \neq 0.$$

5.1. Qubit and coherent state

In terms of this coordinates for quantum qubit state we have

$$|\psi> = \begin{pmatrix} \psi_1 \\ \psi_2 \end{pmatrix} \Rightarrow \frac{1}{\sqrt{1+|\psi|^2}} \begin{pmatrix} 1 \\ \psi \end{pmatrix}.$$

This dermines spin $\frac{1}{2}$ generalized coherent state in terms of stereographic projection of the Bloch sphere to complex plane $\psi \in C$, $\psi = \tan\frac{\theta}{2}e^{i\varphi}$,

$$|\theta, \varphi> = \cos\frac{\theta}{2}|0> + \sin\frac{\theta}{2}e^{i\varphi}|1> .$$

5.2. Symmetric points and symmetric qubits

5.2.1. Symmetric inverse points Points in complex plane ψ and $1/\bar{\psi}$ are symmetrical points with respect to unit circle C around the origin $|\psi| = 1$. As we have seen in the first part, they correspond to positions of hydrodynamic vortex and its image in unit circle bounded domain. Under Möbius transformation generalized circles and corresponding symmetrical points transform to generalized circles and related symmetric points. These symmetric points as projections of $M(x, y, z)$ and $M^*(x, y, -z)$ inverse points on Bloch sphere determine the pair of inverse symmetric qubits $|\theta, \varphi>$ and $|\pi - \theta, \varphi>$ and hence the couple of coherent states

$$|\psi> = \frac{|0> + \psi|1>}{\sqrt{1+|\psi|^2}}, \quad |\frac{1}{\bar{\psi}}> = \frac{\bar{\psi}|0> + |1>}{\sqrt{1+|\psi|^2}}.$$

The unitary Möbius transformation acting on these states produces another couple of symmetric coherent states.

5.2.2. Negative symmetric inverse points Symmetric coherent states are not orthogonal. However if we consider the pair of negative symmetric points ψ and $-\frac{1}{\bar{\psi}}$ being projections of $M(x, y, z)$ and $M^*(-x, -y, -z)$ antipodal points on Bloch sphere, then we have the pair of qubits $|\theta, \varphi>$ and $|\pi - \theta, \varphi>$ and coherent states

$$|\psi> = \frac{|0> + \psi|1>}{\sqrt{1+|\psi|^2}}, \quad |-\frac{1}{\bar{\psi}}> = \frac{-\bar{\psi}|0> + |1>}{\sqrt{1+|\psi|^2}}.$$

These coherent states are orthogonal $< -\frac{1}{\bar{\psi}}|\psi >= 0$. Since Möbius transformation transforms also the pair of negative inverse points (antipodal points) to couple of negative inverse points, the corresponding antipodal quantum states transform in a similar way.

6. Two qubit coherent states

For $\psi \to \infty$ our antipodal points give 0 and ∞ as (negative inverse)symmetric points and corresponding quantum states become orthogonal computational basis states $|1>$ and $|0>$ correspondingly. Then motivated by Bell's states, we can construct the set of orthonormal two qubit coherent states [7], [8]

$$|P_{\pm}>=\frac{1}{\sqrt{2}}\left(|\psi>|\psi>\pm|-\frac{1}{\bar{\psi}}>|-\frac{1}{\bar{\psi}}>\right),$$

$$|G_{\pm}>=\frac{1}{\sqrt{2}}\left(|\psi>|-\frac{1}{\bar{\psi}}>\pm|-\frac{1}{\bar{\psi}}>|\psi>\right).$$

These states are maximally entangled states and the average energy distributions for spin model in these states are surfaces with characteristic extreme points [8].

7. N qubit coherent states

Tensor product of N qubit coherent states can be expanded to computational basis

$$|\psi>^N\equiv\prod_{n=1}^{N}\otimes(|0>+\psi|1>)^n=|00...0>+\psi(|10...0>+...|00...1>) \tag{8}$$

$$+\psi^2(|11...0>+...|00...11>)+...\psi^N|11...1>. \tag{9}$$

It has form of N-degree polynomial with vector coefficients.

7.1. Fibonacci type states

Combination of N qubit states in the form similar to Binet formula gives entangled state

$$|\mathcal{F}_N(\psi)>=\frac{|\psi>^N-|-\psi^*>^N}{\psi-(-\psi^*)}=F_1(\alpha,\beta)(|10...0>+...+|00...1>) \tag{10}$$

$$+F_2(\alpha,\beta)(|11...0>+...+|0...11>)+...+F_N(\alpha,\beta)|11...1>, \tag{11}$$

where coefficients $F_n(\alpha,\beta)$ are complex Fibonacci polynomials.

7.2. Lucas type states

Similar way we get another N qubit entangled state

$$|\mathcal{L}_N(\psi)>=|\psi>^N+|-\psi^*>^N=|00...0>+L_1(\alpha,\beta)(|10...0>+...+|00...1>) \tag{12}$$

$$+L_2(\alpha,\beta)(|11...0>+...+|0...11>)+...+L_N(\alpha,\beta)|11...1>, \tag{13}$$

where coefficients $L_n(\alpha,\beta)$ are complex Lucas polynomials.

8. Complex Fibonacci polynomials

Negative symmetric points with respect to unit circle, ψ and $-\frac{1}{\bar{\psi}}$, are roots of equation

$$\xi^2=(\psi-\frac{1}{\bar{\psi}})\xi+\frac{\psi}{\bar{\psi}}.$$

Substituting $\psi=|\psi|e^{i\phi}$ and $\xi=\eta e^{i\phi}$ we get $\eta^2=a\eta+1$, $a=|\psi|-|\psi|^{-1}$, $\eta^n=\eta F_n(a)+F_{n-1}(a)$ where Fibonacci polynomials are $F_1(a)=1$, $F_2(a)=a$,

$$F_{n+1}(a)=aF_n(a)+F_{n-1}(a).$$

8.1. Binet representation and q-calculus
Fibonacci polynomials can be interpreted as q-numbers with Binet formula

$$F_n(\eta) = \frac{\eta^n - (-\eta)^{-n}}{\eta - (-\eta)^{-1}} = [n]_{\eta,-\eta^{-1}}$$

for negative-symmetrical points as bases [6]. In particular case when $a = 1$ and $|\psi| = \varphi = \frac{1+\sqrt{5}}{2}$ is the Golden Ratio, we have Fibonacci numbers as q-numbers

$$F_n = \frac{\varphi^n - (-\varphi)^{-n}}{\varphi - (-\varphi)^{-1}} = [n]_F.$$

8.1.1. Complex Fibonacci and Lucas polynomials Recursion formula for complex Fibonacci polynomials is

$$F_{n+1}(\alpha,\beta) = \alpha F_n(\alpha,\beta) + \beta F_{n-1}(\alpha,\beta),$$

where $\alpha = \psi - \bar{\psi}^{-1}$, $\beta = \psi/\bar{\psi}$. They are related to real Fibonacci polynomials by

$$F_n(\alpha,\beta) = F_n(a)e^{i\phi(n-1)},$$

where $\phi = arg\,\psi$. In a similar way for complex Lucas polynomials we have

$$L_n(\alpha,\beta) = \psi^n + (-\bar{\psi})^{-n}$$

and

$$L_n(\alpha,\beta) = L_n(a)e^{i\phi n}.$$

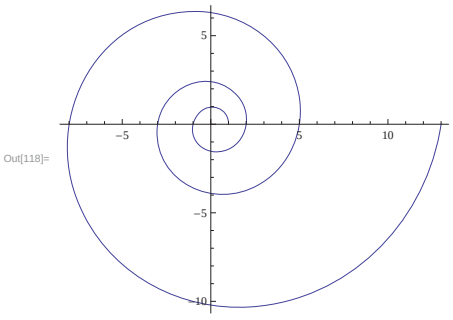

Figure 2. Complex Fibonacci spiral: $\phi = \pi$.

8.2. Complex Fibonacci curve
We can draw the set of these polynomials as points in complex plane. For $a = 1 \rightarrow \varphi = \frac{1+\sqrt{5}}{2}$ we introduce the Fibonacci spiral curve

$$\mathcal{F}_(t) = F(t)e^{i\phi(t-1)} = \frac{\varphi^t - (-\varphi)^{-t}}{\sqrt{5}} e^{i\phi(t-1)}.$$

It is parametric curve with

$$x(t) = \frac{1}{\sqrt{5}}[e^{t\ln\varphi}\cos(\phi(t-1)) - e^{-t\ln\varphi}\cos(\pi t + \phi(t-1))],$$

$$y(t) = \frac{1}{\sqrt{5}}[e^{t\ln\varphi}\sin(\phi(t-1)) - e^{-t\ln\varphi}\sin(\pi t + \phi(t-1))].$$

We draw these spiral curve on Figure 2 for $\phi = \pi$. It is rotating anticlockwise in such a way that intersect x axis at points distant from origin as Fibonacci sequence. To have more fast rotation around the curve In Figures 3-8 we choose $\phi = 100\pi$. Then to produce Fibonacci sequence after every 50 rotation, the curve shows reach set of patterns with interesting shapes.

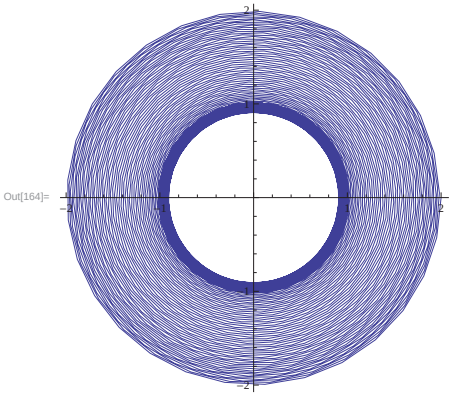

Figure 3. Complex Fibonacci spiral $\phi = 100\pi$: t=3.

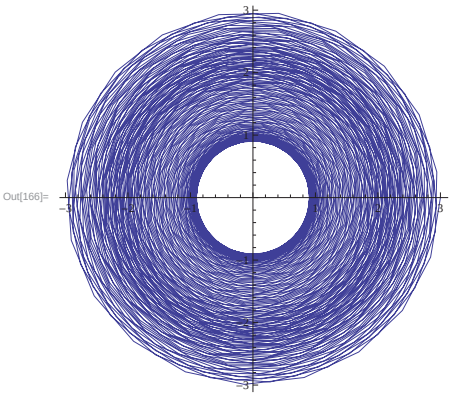

Figure 4. Complex Fibonacci spiral $\phi = 100\pi$: t=4.

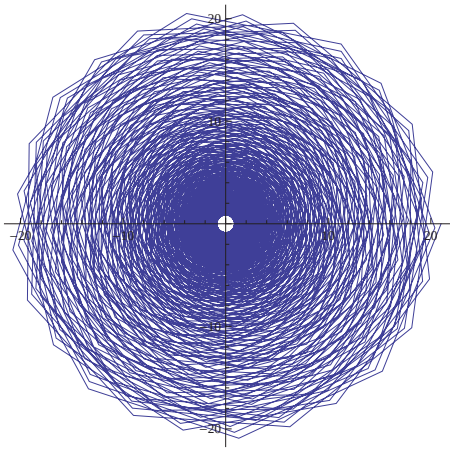

Figure 5. Complex Fibonacci spiral $\phi = 100\pi$: t=8.

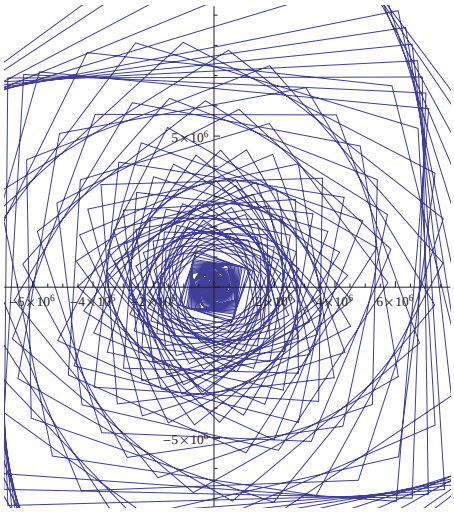

Figure 6. Complex Fibonacci spiral $\phi = 100\pi$: t=50.

8.3. Acknowledgments
This work was supported by Izmir Institute of Technology and by TUBITAK Grant (Project TBAG No. 110T679).

References

[1] Poincare H 1893 *Theorie des Tourbillions* (Paris: Georges Carre)
[2] Pashaev O K and Yilmaz O 2008 *J. Phys. A. Math Theor* **41** 135207
[3] Pashaev O K and Yilmaz O 2011 *J. Phys. A. Math Theor* **44** 185501
[4] Milne-Thomson L M 1968 *Theoretical Hydrodynamics* (London: Macmillan)
[5] Erzan A and Eckmann J P O 1997 *Phys. Rev. Lett.* **78** 3245-8
[6] Pashaev O K and Nalci S 2012 *J. Phys. A. Math Theor* **45** 015303
[7] Pashaev O K 2012 *J. Phys.: Conf. Series* **343** 012093
[8] Pashaev O K and Gurkan N 2012 *New Journal of Physics* **14** 063007
[9] Akhiezer N I 1990 *Elements of the Theory of Elliptic Functions* (Moscow: AMS)
[10] Vitiello G 2008 Topological defects, fractals and the structure of quantum field theory *Preprint* hep-th/0807.2164v1; 2012 math-ph/1206.1854v1

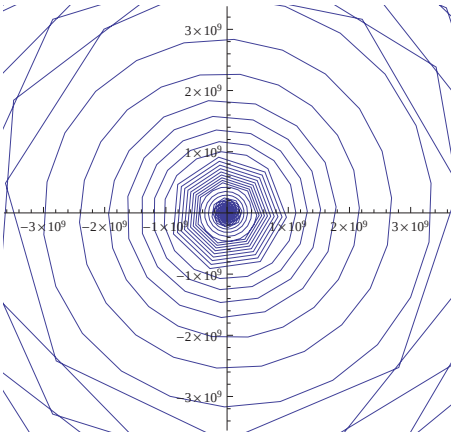

Figure 7. Complex Fibonacci spiral $\phi = 100\pi$: t=70.

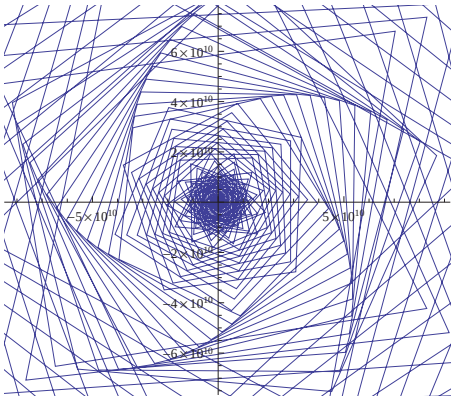

Figure 8. Complex Fibonacci spiral $\phi = 100\pi$: t=80.

[11] Vitiello G 2012 Fractals, coherent states and self-similarity induced noncommutative geometry *Preprint* math-ph/1206.1854v1